Implicit Finite-Difference Computations of Unsteady Transonic Flows about Airfoils

W. F. Ballhaus*
NASA Ames Research Center and Aeromechanics Laboratory, U.S. Army Aviation R&D Command, Moffett Field, Calif.
and
P. M. Goorjian*
Informatics Corporation, Palo Alto, Calif.

A computer code, LTRAN2, has been constructed that efficiently computes low-frequency unsteady transonic flows about airfoils in motion. The code solves the two-dimensional, nonlinear, low-frequency, small-disturbance equation by an alternating-direction implicit (ADI) algorithm. The underlying theory of the governing equation and the construction of the solution algorithm are discussed. As a check on the code, solutions computed for the linear low-frequency small-disturbance equation are compared with known answers from linear theory. Then nonlinear results are presented, and Tijdeman's experimental observations of shock wave motions resulting from airfoil flap oscillations are qualitatively reproduced computationally. These computations compare favorably with those of Magnus and Yoshihara and are obtained in substantially less computer time.

Introduction

THIS effort is a step toward the development of computational methods for predicting unsteady loads on aerodynamic bodies and for providing an understanding of the physics of unsteady transonic flows in engineering applications. The objective was to construct a simple, efficient algorithm for computing the unsteady transonic flowfield about an airfoil in unsteady motion. Emphasis has been placed on the efficient treatment of low-frequency oscillatory flows. These flows are of interest because shock excursion amplitudes, and hence unsteady aerodynamic force amplitudes, usually increase with decreasing frequency for a fixed airfoil oscillatory motion amplitude.

In the design of a computer simulation method for unsteady transonic flows, the following features must be considered: 1) treatment of nonlinear unsteady effects, including shock wave motions, 2) computational efficiency, 3) treatment of arbitrary airfoils and airfoil motions, and 4) treatment of three-dimensional and viscous effects. Solution methods reported to date are deficient in one or more of these areas.

Time-linearized methods for unsteady transonic flows[1-5] do not presently treat shock motions correctly. Their application is restricted to very small amplitude airfoil motions that constrain the shock waves to their steady-state position. However, these methods can be used to provide input for aeroelastic computations for which only infinitesimal amplitude motions need be considered. Finite-difference schemes that integrate the equations of motion in time[6-13] are capable of simulating nonlinear, unsteady transonic flow phenomena correctly, including shock wave motions (for a reivew of unsteady transonic flow methods, see Ref. 14). Since these schemes usually rely on shock capturing to resolve shock waves, the governing equations must be solved in conservation form, which is not always convenient. Failure to maintain proper conservation form can result in computed shock speeds that depend on grid spacing.

Presented as Paper 77-205 at the AIAA 15th Aerospace Sciences Meeting, Los Angeles, Calif., Jan. 24-26, 1977; submitted Feb. 1, 1977; revision received Sept. 6, 1977.

Index categories: Transonic Flow; Nonsteady Aerodynamics; Computational Methods.

*Research Scientist. Member AIAA.

Time integration methods are computationally efficient when integration time steps are chosen on the basis of accuracy. For low-frequency motions, relatively large time steps can be used with no appreciable sacrifice in flowfield resolution; for higher frequency motions, smaller time steps must be taken. Explicit finite-difference schemes[8,15] applied to low-frequency transonic flows, however, have a time-step restriction for stability that is substantially more severe than that required for accuracy. This difficulty was partially overcome by the use of semi-implicit schemes,[9] which have much less severe time step restrictions. More recently, fully implicit schemes[7,10] have been developed that permit time-step selection based on accuracy rather than stability considerations.

Simple treatment of arbitrary airfoils and airfoil motions is the principal advantage of transonic small-disturbance formulations. The airfoil boundary condition is imposed, in terms of airfoil slopes, on a flat, mean-surface approximation to the airfoil. In less approximate formulations, coordinate mappings are usually required, and it may be necessary to retransform for each time-step. However, the assumptions that permit this simplification place some restrictions on the airfoil thickness-to-chord ratios and motion amplitudes that can be treated. Often, though, the small-disturbance assumptions are no more restrictive than the assumption of inviscid flow, i.e., both viscous and non-small-disturbance effects become increasingly important with increasing angle of attack and airfoil thickness ratio.

Three-dimensional and viscous influences are usually important in transonic flow applications. However, the inclusion of these effects is beyond the scope of the present effort. Small-disturbance formulations have been successfully applied to steady three-dimensional transonic flows (e.g., see Ref. 16) and should be extendible to unsteady three-dimensional flows. Simple models could also be added to provide some correction for viscous effects. For example, approximate treatment of the effect of a boundary layer on the motion of a shock wave could be included in the present formulation by using the model described in Ref. 15.

The method described here uses a conservative, implicit finite-difference algorithm to time-accurately integrate the nonlinear, low-frequency transonic small-disturbance equation. The computer code, LTRAN2, was developed for application to arbitrary combinations of airfoil pitch, plunge,

and flap deflections. Unsteady solutions can be computed in about one minute of CDC 7600 computer time. Results are compared with results from linear theory and other computational methods. Also presented are solutions that illustrate the three types of shock wave motion, observed experimentally by Tijdeman,[17] for an airfoil with oscillating trailing-edge flap.

Governing Equation and Boundary Conditions

Governing Equation

The unsteady, transonic small-disturbance equation can be written

$$A\phi_{tt} + 2B\phi_{xt} = C\phi_{xx} + \phi_{yy} \tag{1}$$

where

$$A = k^2 M_\infty^2 / \delta^{2/3}$$

$$B = kM_\infty^2 / \delta^{2/3}$$

$$C = (1 - M_\infty^2)/\delta^{2/3} - (\gamma + 1) M_\infty^m \phi_x$$

and where ϕ is the disturbance velocity potential, M_∞ is the freestream Mach number, and δ is the airfoil thickness-to-chord ratio. The choice of the exponent m is somewhat arbitrary. In this report, m is a function of M_∞ chosen to adjust the critical pressure coefficient, C_p^*, for Eq. (1) to match the exact isentropic C_p^*.[14] The parameter k is the reduced frequency. For an airfoil of chord length c, traveling with speed U_∞, and executing some unsteady oscillatory motion of frequncy ω, $k \equiv \omega c / U_\infty$. The reduced frequency is given in terms of radians of oscillatory motion per chord length of airfoil travel. The quantities x, y, t, ϕ in Eq. (1) have been scaled by $c, c/\delta^{1/3}, \omega^{-1}, c\delta^{2/3} U_\infty$, respectively. The right-hand side of Eq. (1) is the familiar two-dimensional, transonic, small-disturbance equation for steady flows.

An approximation to Eq. (1), valid for low reduced frequencies, is the equation

$$2B\phi_{xt} = C\phi_{xx} + \phi_{yy} \tag{2}$$

where B and C are defined in Eq. (1). This equation can be derived from the unsteady Euler equations under the assumptions

$$k \sim \delta^{2/3} \sim 1 - M_\infty^2 \ll 1 \tag{3}$$

The pressure coefficient expression consistent with Eq. (3) is $C_p = -2\delta^{2/3}\phi_x$.

To understand the implications of the low-frequency approximation, it is helpful to investigate its effect on the characteristic surfaces, the wave fronts along which information is propagated throughout the flowfield. Suppose that, at $t = 0$, an instantaneous disturbance of infinitesimal strength occurs at the point $x = y = 0$ in some uniform stream with velocity u and sound speed a. The characteristic equation for Eq. (1) is

$$ct^2 - Ax^2 - (AC + B^2) y^2 + 2Bxt = 0 \tag{4}$$

and so, for $t > 0$, the disturbance front is given by

$$\left(x - \frac{Bt}{A}\right)^2 + \left(\frac{AC + B^2}{A}\right) y^2 = \left(\frac{AC + B^2}{A^2}\right) t^2 \tag{5}$$

If we drop the scaling on t, ϕ, and y and replace M_∞ by u/a, Eq. (5) can be written

$$(x - ut)^2 + y^2 = a^2 t^2 \tag{6}$$

The disturbance front propagates at the speed of sound relative to the fluid. It is a circle with radius $(a \cdot t)$ and center at $x = ut$, $y = 0$, as shown in Fig. 1. The disturbance center corresponds to the location of the fluid particle that was at the point of the disturbance at $t = 0$, and it moves with velocity u. In the plane $y = 0$, the effect of the disturbance propagates upstream, for $u < a$, with velocity $(u - a)$, and downstream with velocity $(u + a)$.

Taking $A = 0$ in Eq. (5) gives a relation that is similar to Eq. (6) and that describes the disturbance front that corresponds to the low-frequency equation, Eq. (2):

$$y^2 = \frac{2a^2 t}{u}\left[x + \left(\frac{a+u}{2u}\right)(a-u)t\right] \tag{7}$$

The disturbance front is a parabola, as illustrated in Fig. 2. Note that the disturbance propagation rate in the downstream direction is infinite. In the low-frequency approximation, the sound and particle speeds are infinite.[14] Hence, the downstream propagation rate, which is the sum of the two, is also infinite. However, the upstream propagation rate, the difference of the two, is finite and equal to $(u - a)(u + a)/2u$. Since $u \sim a$ for transonic flows, this a good approximation to the upstream propagation rate $(u - a)$ corresponding to Eq. (1).

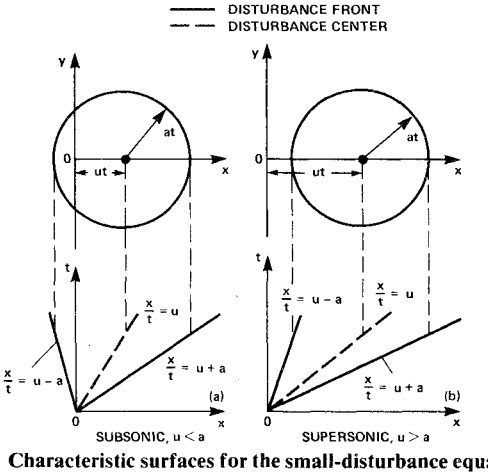

Fig. 1 Characteristic surfaces for the small-disturbance equation.

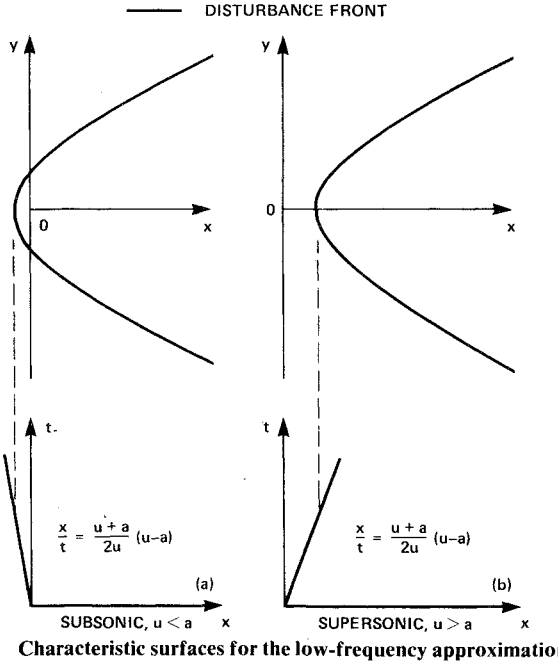

Fig. 2 Characteristic surfaces for the low-frequency approximation.

The low-frequency approximation assumes that the time scale of the motion is of the same order as the time scale associated with upstream disturbance propagation and that these scales are much larger than the time scales associated with downstream propagation and convection, that is

$$1/\omega \sim c/(u-a) \gg c/(u+a) \sim c/u \tag{8}$$

Hence, for transonic flows ($u \sim a$), the low-frequency condition is $k \equiv \omega c/u \ll 1$.

Boundary Conditions

In small-disturbance formulations, the condition of no flow through the airfoil surface is usually satisfied on a straight-line, mean-surface approximation to the airfoil. Here, the condition

$$\phi_y(x,0,t) = f'(x,t) \quad 0 \le x \le 1 \tag{9}$$

is specified, where $\delta f'(x,t)$ is the local instantaneous airfoil slope.

In the solution of Eq. (1) for lifting airfoils, a constant jump in potential across the vortex sheet, $y=0$, must be enforced along freestream particle paths downstream of the airfoil. In the low-frequency formulation, the jump in potential can be assumed uniform in x from the airfoil trailing edge to downstream infinity, as in the steady case; that is, the downstream flow adjusts instantaneously to changes in the lift on the airfoil. The reason is that the rate of change in lift due to the (low-frequency) motion of the airfoil is much smaller than the rate at which the effect of these changes is propagated downstream.

In the far field, ϕ_x and ϕ_y approach zero as the distance from the airfoil approaches infinity.

Solution Algorithm

Alternating-Direction Implicit Scheme

The solution, in terms of the disturbance velocity potential, is obtained for each grid point in the flowfield by using the alternating-direction implicit scheme (ADI) described in Ref. 10 to solve the low-frequency transonic equation, Eq. (2). The solution is advanced from time level n to level $n+1$ by the following two-step procedure:

x-sweep:

$$2B(\Delta t)^{-1}\delta_x(\tilde{\phi}^{n+1}_{j,k} - \phi^n_{j,k}) = D_x f_{j,k} + \delta_{yy}\phi^n_{j,k} \tag{10a}$$

y-sweep:

$$2B(\Delta t)^{-1}\delta_x(\phi^{n+1}_{j,k} - \tilde{\phi}^{n+1}_{j,k}) = \tfrac{1}{2}\delta_{yy}(\phi^{n+1}_{j,k} - \phi^n_{j,k}) \tag{10b}$$

where

$$B = kM_\infty^2/\delta^{2/3} \tag{10c}$$

$$\delta_x\phi_{j,k} = \underset{\text{(first order)}}{2(\phi_{j,k} - \phi_{j-1,k})(x_{j+1} - x_{j-1})^{-1}}$$
$$= \underset{\text{(second order)}}{(3\phi_{j,k} - 4\phi_{j-1,k} + \phi_{j-2,k})(x_{j+1} - x_{j-1})^{-1}} \tag{10d}$$

$$\delta_{yy}\phi_{j,k} = 2[(\phi_{j,k+1} - \phi_{j,k})(y_{k+1} - y_k)^{-1}$$
$$- (\phi_{j,k} - \phi_{j,k-1})(y_k - y_{k-1})^{-1}](y_{k+1} - y_{k-1})^{-1} \tag{10e}$$

$$f_{j,k} = \tfrac{1}{2}[C^n_{j,k}\phi^{n+1}_{x_{j,k}} + (1 - M_\infty^2)\phi^n_{x_{j,k}}/\delta^{2/3}] \tag{10f}$$

$$C^n_{j,k} = (1 - M_\infty^2)/\delta^{2/3} - (\gamma+1)M^m_\infty\phi^n_{x_{j,k}} \tag{10g}$$

$$\phi_{x_{j+\frac{1}{2},k}} = (\phi_{j+1,k} - \phi_{j,k})(x_{j+1} - x_j)^{-1} \tag{10h}$$

$$D_x f_{j,k} = 2(x_{j+1} - x_{j-1})^{-1}[(1-\epsilon_j)(f_{j+\frac{1}{2},k} - f_{j-\frac{1}{2},k})$$
$$+ \epsilon_{j-1}(f_{j-\frac{1}{2},k} - f_{j-3/2,k})] \tag{10i}$$

$$\epsilon_j = [{}^{0}_{1}] \text{ for } (C^n_{j+\frac{1}{2},k} + C^n_{j-\frac{1}{2},k})[{}^{\geq}_{<}]0 \tag{10j}$$

The scheme is either first- or second-order accurate depending on the choice of the operator δ_x. The first-order operator has been used for all of the computed results reported here because of its superior shock-capturing characteristics. The subscripts j and k are grid-point indices in the x and y directions, respectively, and Δt is the integration time step. Use of the mixed-difference operator D_x is required to maintain stability for both subsonic and supersonic flow regions.

Special care must be taken in the construction of the D_x and δ_x operators to maintain conservation form for cases with nonuniform grid spacing. Conservation form must be maintained in the difference equation for the proper treatment of shock waves. Otherwise, shock speeds can depend on the grid spacing. Furthermore, variations in grid spacing must be smooth to maintain accuracy.

Note that the solution algorithm is noniterative. That is, the solution for the $n+1$ time level is obtained directly after two sweeps through the grid. On the x-sweep, a matrix is generated that is lower tridiagonal for supersonic points ($\epsilon_{j-1} = \epsilon_j = 1$) and tridiagonal for subsonic points ($\epsilon_{j-1} = \epsilon_j = 0$). A quadradiagonal solver is used that solves the matrix equation for $\tilde{\phi}^{n+1}_{j,k}$ like the Thomas algorithm for tridiagonal matrix equations. On the y-sweep, the only x differences are in the δ_x operator, which is backward differenced. Hence, the scheme is marched from upstream to downstream by solving a tridiagonal matrix equation for each x = constant line of y grid points.

The ADI scheme has no Δt restriction based on a linear stability analysis. However, an instability can be generated by the motion of shocks across which the differencing switches from backward to central. To prevent this instability from occurring, Δt must be chosen small enough that such shock waves do not move a distance greater than one spatial grid point per time step. This restriction is necessary to maintain accuracy anyway, and it is orders of magnitude less severe than the Δt restrictions associated with explicit, or even semi-implicit, methods applied to low-frequency flows.

Grid System and Boundary Conditions

The difference equation is solved on a Cartesian grid system surrounding the airfoil. Grid points are clustered in the leading- and trailing-edge regions in x and near the airfoil in y. The grid spacing is smoothly stretched, with distance from the airfoil such that the grid boundaries are located about 1,000 chord lengths away from the airfoil.

On the x-sweep, the intermediate solution $\tilde{\phi}^{n+1}_{j,k}$ is obtained for each y = constant line, and it is independent of $\tilde{\phi}^{n+1}_{j,k}$ on any other line. Values of ϕ^n and $\tilde{\phi}^{n+1}$ are stored on the line $y=0$ in separate arrays ϕ^U_j, ϕ^L_j, and $\tilde{\phi}^U_j$, $\tilde{\phi}^L_j$. On the airfoil surface, the δ_{yy} operator contains the Neumann boundary condition, Eq. (9), and ϕ^U_j and ϕ^L_j for the upper and lower surfaces, respectively. Downstream of the airfoil on $y=0$, the condition $\phi^U_j = \phi^L_j + \Gamma^n$ is incorporated into the δ_{yy} operator. Here Γ^n is the circulation, which varies as a function of time.

On the y-implicit sweep, because $\phi^{n+1}_{j,k}$ is stored in separate (upper and lower) arrays on $y=0$, nontridiagonal matrix equations are generated in the region upstream from the airfoil. There the matrix equation can be made tridiagonal by using the two difference equations for ϕ^U_j and ϕ^L_j to eliminate either unknown. On the airfoil surface, the matrix equations for the regions above and below the airfoil are decoupled. In that region, the solution $\phi^{n+1}_{j,k}$ for each x = constant line can be obtained either by solving two matrix equations or by masking one region from the other and solving one matrix equation. Downstream from the airfoil, either ϕ^U_j or ϕ^L_j can be eliminated because their difference is equal to Γ^{n+1}.

The circulation at the new time level, Γ^{n+1}, must be computed before points downstream of the airfoil can be updated. It can be obtained without iteration, by the expression

$$\Gamma^{n+1} = (\phi^U_{JTE} - \phi^L_{JTE})^{n+1} \tag{11}$$

where JTE is the value of the j index of the grid point on the airfoil nearest the trailing edge. Equation (11) can be derived by first assuming that the trailing edge is located midway between x_{JTE} and x_{JTE+1}. Then, matching the upper and lower surface pressure coefficients at the trailing edge gives

$$\phi^U_{j+1} - \phi^U_j = \phi^L_{j+1} - \phi^L_j \quad \text{for } j = JTE \tag{12}$$

The point $j = JTE+1$ lies downstream of the airfoil, and therefore

$$\phi^U_{JTE+1} = \phi^L_{JTE+1} + \Gamma^{n+1} \tag{13}$$

Combining Eqs. (12) and (13) gives Eq. (11). Note that, since the y-sweep is marched in increasing j, the new circulation Γ^{n+1} is obtained from ϕ_{JTE} values and then applied to find ϕ_j for $j > JTE$.

Correct specification of the boundary condition at the outer mesh boundaries should yield the same solution near the airfoils as though the computational domain were infinite. To determine the correct conditions to specify there, one would have to properly account for the time history of the circulation and how its effect has been propagated throughout the flowfield. Because this is a formidable task, a simple alternative approach is used here. The grid boundaries are located about 1000 chord lengths away from the airfoil. The mean-steady-state far-field solution is specified on all boundaries but $x = x_{JMAX}$, the downstream boundary. There the condition $\phi_{JMAX,k} = \phi_{JMAX-2,k}$ (i.e., $\phi_{xJMAX} = 0$) is enforced in the implicit solution procedure. This allows the unsteady potential jump across the vortex sheet at $x_j = x_{JMAX}$ to adjust to the changing circulation. Numerical experiments have been performed that indicate that the circulation is insensitive to the boundary conditions applied in this manner.

Computed Results

Comparisons with Linear Theory

Computed results from LTRAN2 are compared first with exact linear theory results. This is to establish the capability of the finite-difference algorithm to provide accurate unsteady solutions. The linear theory results are solutions to Eq. (1) with $\gamma = -1$ in the expression for C. The linear LTRAN2 results are solutions to the low-frequency equation, Eq. (2), also with $\gamma = -1$. Differences in the comparison can be attributed to two factors: 1) numerical error in the algorithm and 2) deficiencies in the low-frequency approximation. These deficiencies result from neglecting ϕ_{tt} in the governing equation, from the simplified treatment of the wake, and from neglecting ϕ_t in the expression for the pressure coefficient.

All of the LTRAN2 computations reported in this section were computed using a 99,79 grid in the x,y directions, unless otherwise noted. Integration time steps for the linear case normally were $\Delta t = 3°$, corresponding to 120 time steps per cycle of oscillatory motion. Unsteady computations were initiated by using a steady-state relaxation solution. The equations were then integrated in time for several cycles until the solution became periodic.

Figure 3 compares computed and exact linear theory lift and midchord moment coefficients, normalized by the amplitude, for an oscillatory plunging airfoil. The comparison is for a range of reduced frequencies at fixed freestream Mach numbers. For all Mach numbers considered, the agreement is good for the lower frequencies. The moment coefficient results show unexpectedly good agreement over the entire reduced-frequency range included. Note that phase-lags increase with increasing Mach number because of the slower upstream disturbance propagation rate at higher Mach numbers. The low-frequency results generally agree better with linear theory for the higher Mach numbers, which is

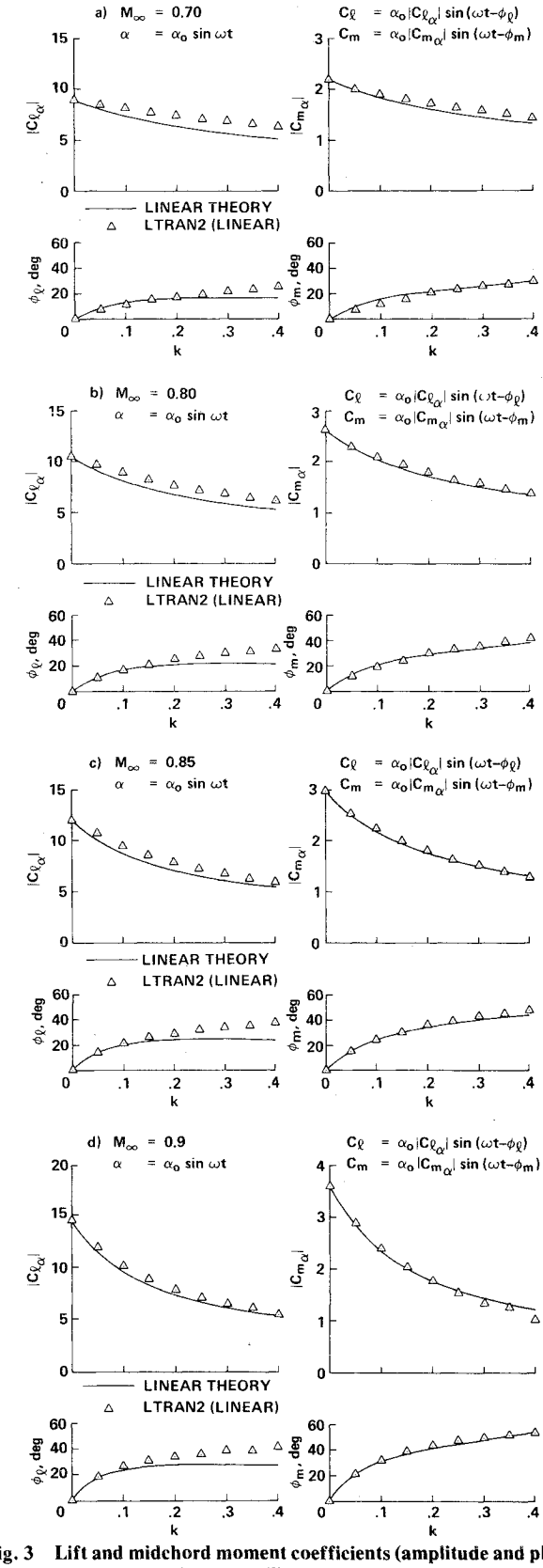

Fig. 3 Lift and midchord moment coefficients (amplitude and phase) vs reduced frequency for an oscillatory plunging airfoil, $k = \omega c/U_\infty$. a) $M_\infty = 0.70$, b) $M_\infty = 0.80$, c) $M_\infty = 0.85$, d) $M_\infty = 0.9$.

consistent with the assumptions, Eq. (3), under which the low-frequency approximation is derived. (The authors are indebted to Dr. Sanford Davis of Ames Research Center for supplying the linear theory results shown in Fig. 3.)

Midchord pitching moment results as a function of freestream Mach number are shown in Fig. 4 for plunging oscillations of an NACA 64A006 airfoil at a reduced frequency of 0.1. The agreement between linear LTRAN2 computations and exact linear theory is excellent. In the linear case, the pitching moment dependency on Mach number is very weak, and the (normalized) pitching moment is independent of airfoil shape or oscillation amplitude. This is not true for the nonlinear case, in which the pitching moment clearly depends strongly on M_∞. Nonlinear LTRAN2 computed results are shown for three oscillation amplitudes. The differences in the three results are indications of nonlinear unsteady behavior which, incidentally, cannot be treated by time-linearized methods.[1-5] For some of these computations at the larger amplitudes, the time step was reduced to 1.5° to avoid the nonlinear instability referred to in our discussion of the solution algorithm.

An as yet unexplained difficulty was encountered in the nonlinear case $M_\infty = 0.89$ for the 0.5° amplitude case; a symmetric periodic solution could not be obtained. Symmetric periodic solutions were obtained for the 1.5° amplitude case in about 2.5 cycles, and for the 1° case in about 7 cycles. However, at 0.5°, the lift and moment became periodic about nonzero mean values that depended on the initial conditions.

Computed results are compared with linear theory results in terms of upper and lower surface pressure-coefficient differences for an airfoil with oscillating trailing-edge flap in Fig. 5. (The solutions should be independent of airfoil shape in this linear case.) The computed results are from LTRAN2 by solving the linear form of Eq. (2) and from Ehlers[1] for the linear form of Eq. (1). The linear (flat-plate) theory results were obtained from the National Aerospace Laboratory, The Netherlands. The LTRAN2 results agree reasonably well with linear theory in both magnitude and phase.

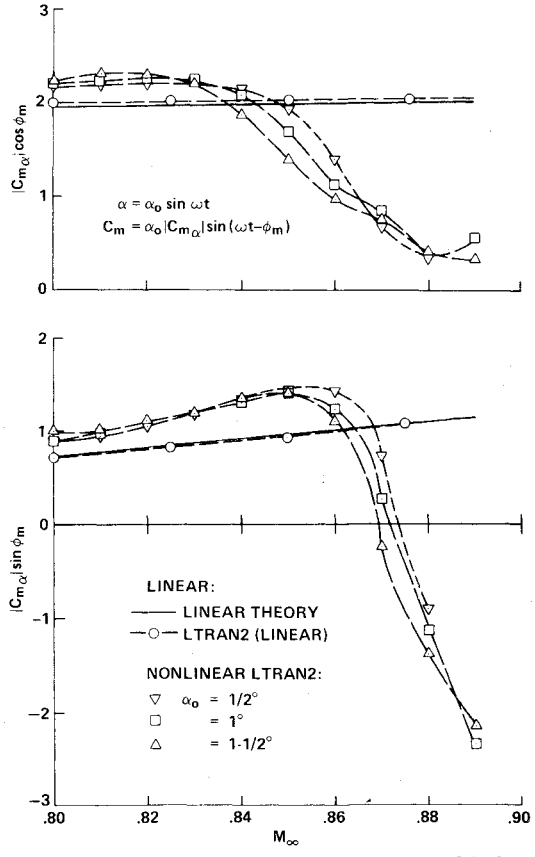

Fig. 4 Midchord moment coefficients vs free-stream Mach number for an oscillatory plunging NACA 64A006 airfoil, $k = \omega c/U_\infty = 0.1$.

Nonlinear Computations for the Oscillating Flap Case

Here, LTRAN2 solutions are presented for the oscillating-flap airfoil shown in Fig. 5. Qualitative comparisons with the experimental observations of Tijdeman, and quantitative comparisons with the computed results of Magnus and Yoshihara demonstrate the capability of the present algorithm to properly resolve shock wave motions.

Tijdeman[17] has identified three types of periodic shock wave motion that result from sinusoidal flap motion of the airfoil shown in Fig. 5.

In type A, *sinusoidal shock wave motion*, the shock moves nearly sinusoidally (only the lowest harmonic was measured) but with a phase shift relative to the flap motion. There also exists a phase shift between the shock motion and its strength; that is, the maximum shock strength is not encountered when the shock reaches its maximum downstream location, as in the steady case, but at a later time during its upstream motion.

In type B, *interrupted shock wave motion*, the shock moves as in type A, but now the oscillatory shock strength is of the same magnitude as the mean steady shock strength. Hence, the shock weakens so that it disappears during the downstream-moving portion of its cycle.

Type C, *upstream propagating shock waves*, occurs at slightly supercritical conditions. Shock waves are formed periodically that do not oscillate in displacement but continue to propagate upstream as the embedded supersonic region vanishes during the flap motion cycle.

Time-integration solutions to the unsteady Eulerian equations have recently been reported by Magnus and

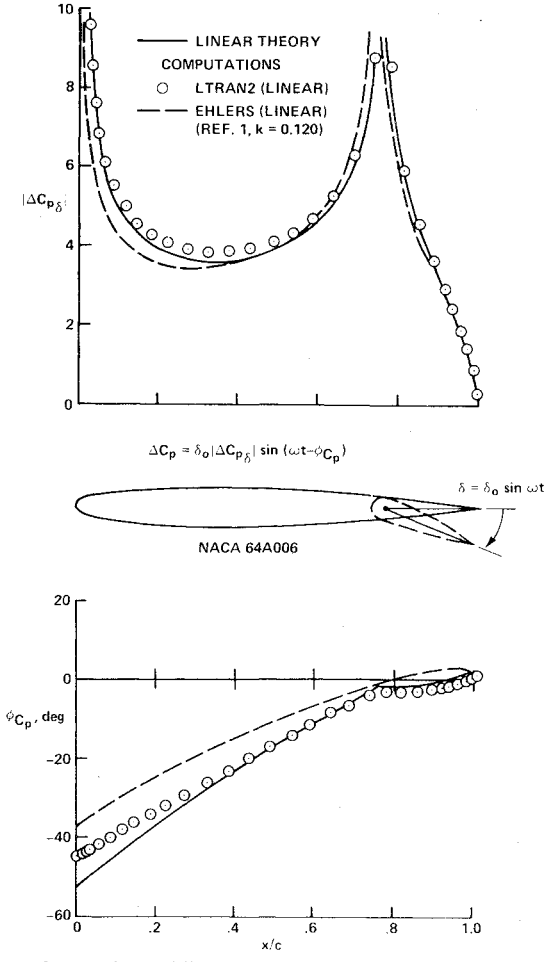

Fig. 5 Comparison of linear pressure coefficient differentials across an airfoil with oscillating trailing-edge flap, $M_\infty = 0.80$, $k = 0.128$.

Yoshihara[15] for the oscillating flap case. We are grateful to them for supplying the solutions shown in Figs. 6 and 7.

Type A motion is illustrated in Fig. 6, and the results are qualitatively similar to Tijdeman's experimental observations. Note the phase shift between the computed shock wave location and the flap motion. The maximum downstream shock excursion does not occur when the flap reaches its maximum downward deflection, as in the steady case. Note also that the shock strength is not in phase with the shock displacement. The maximum shock strength corresponds to a time between E and F, while the maximum downstream displacement corresponds to a time near D. The maximum downward flap deflection corresponds to a time between B and C.

Type B motion is illustrated in Fig. 7. The shock reaches its maximum downstream extent at time D, increases in strength at time E, and then weakens at times F and A so that it totally disappears at time B. The shock reappears at time C and strengthens as it moves again downstream to its location at time D. LTRAN2 and Magnus-Yoshihara results agree reasonably well throughout the cycle. Detailed comparisons at the points where the shock is strongest ($\omega t = 230°$) and weakest ($\omega t = 50°$) are shown in Fig. 8.

The LTRAN2 and Magnus-Yoshihara results agree better than might be expected for the high reduced frequencies involved ($k = 0.468, 0.358$). A possible explanation is that the characteristic length used in the expression for reduced frequency is incorrectly, in this case, taken to be the chord length, c. Fluctuations in the flowfield occur primarily in the region between the shock wave and the trailing edge, a distance that is more nearly equal to the flap length, $c/4$ than to the chord length. Including $c/4$ as the proper length scale in the expression for reduced frequency gives $k = \omega c/4U_\infty = 0.117$ and 0.0895 for the cases shown in Figs. 6 and 7, respectively. These values are well within the low reduced frequency range, which, from our experience, is bounded by $k \approx 0.2$.

Type C motion is illustrated in Fig. 9. A shock wave forms at some time between C and D, then strengthens and propagates upstream. The forward motion of the shock wave entirely eliminates the embedded supersonic region at some time between E and F. The upper surface flow is entirely

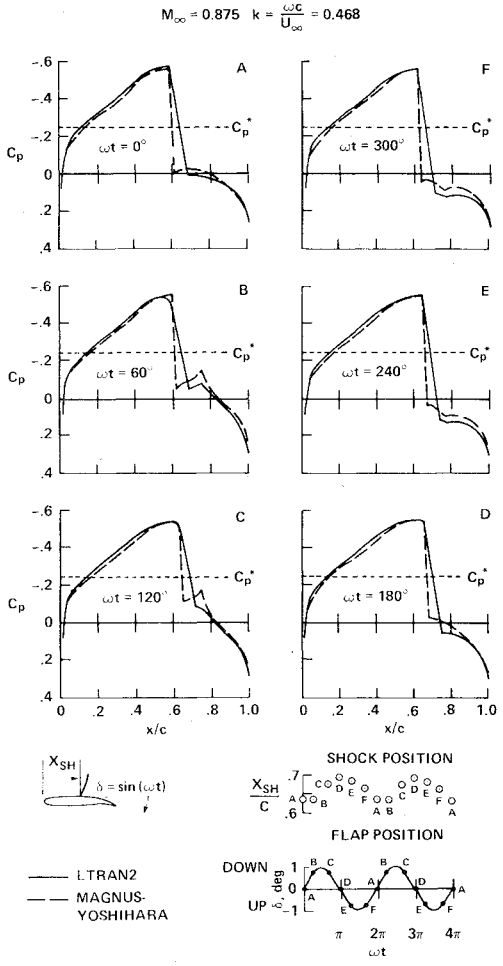

Fig. 6 Unsteady upper surface pressure coefficients for an NACA 64A006 airfoil with oscillating trailing-edge flap, type A motion.

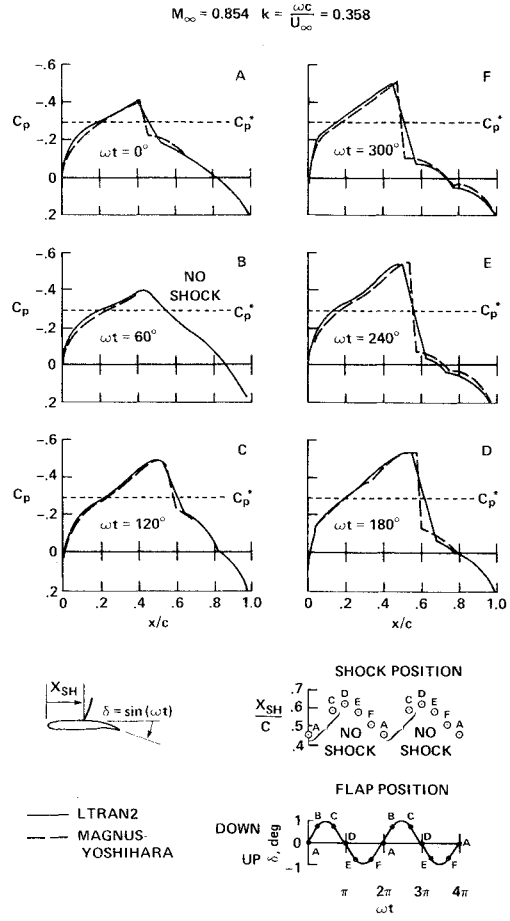

Fig. 7 Unsteady upper surface pressure coefficients for an NACA 64A006 airfoil with oscillating trailing-edge flap, type B motion.

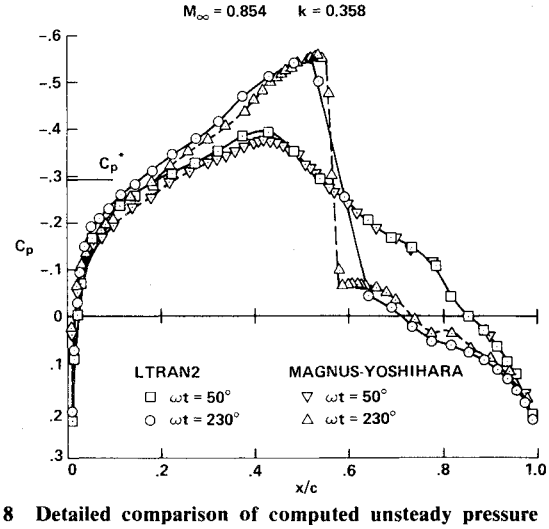

Fig. 8 Detailed comparison of computed unsteady pressure coefficients for type B motion.

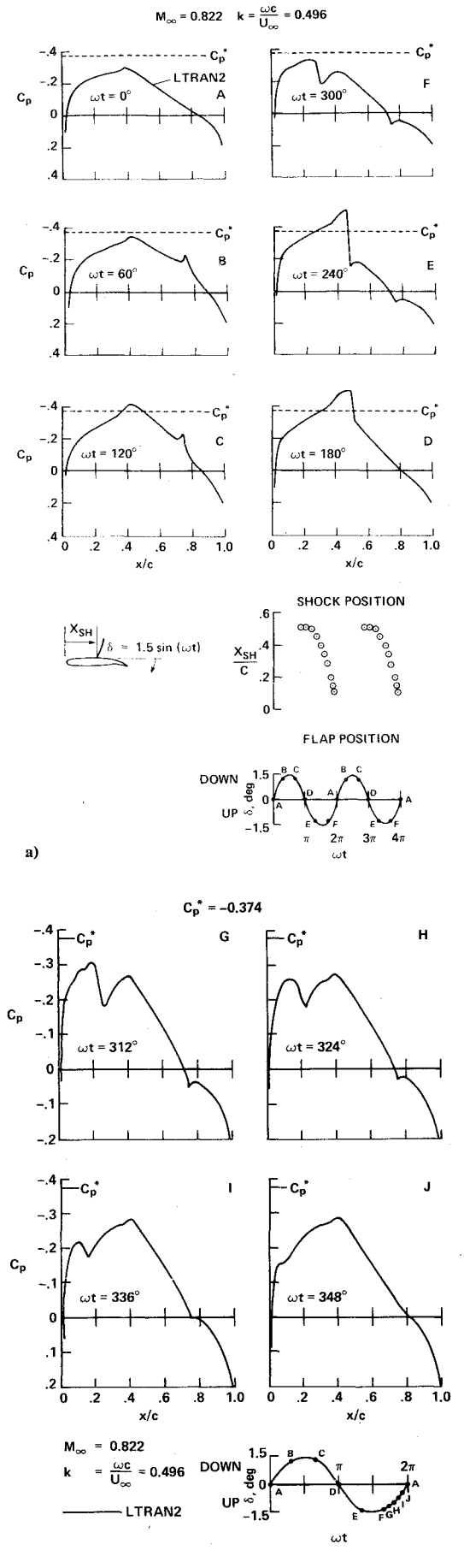

Fig. 9 Unsteady upper surface pressure coefficients for an NACA 64A006 airfoil with oscillating trailing-edge flap, type C motion.

subsonic from this time until some time just before C. The shock wave continues to propagate upstream as shown at times G, H, and I. At time J, it has disappeared, probably dissipated by numerical viscosity. A fine x-grid spacing of 1% chord was used to improve the resolution of the shock wave in this case. Type C shock motion has been computed for a different airfoil motion in Ref. 10 (also reported in Ref. 14). In this case, the shock was clearly resolved as it traveled several chord lengths upstream from the airfoil after having propagated off the leading edge.

The type A, B, and C cases shown were all computed for freestream Mach numbers that were lower than the corresponding Mach numbers in Tijdeman's experiments. Wind-tunnel interference effects and viscous effects would have to be modeled for the computations to reliably reproduce the experimental results for the same Mach numbers.

Concluding Remarks

An implicit, finite-difference algorithm has been developed for the efficient solution of low-frequency unsteady transonic flows. Solutions can be obtained in substantially less computer time than required for explicit algorithms. For example, the implicit algorithm applied to the low-frequency equation, Eq. (2) consumed eight seconds of CDC 7600 computer time per cycle of oscillatory motion to generate the type B motion solution shown in Fig. 7. The Magnus-Yoshihara procedure, an explicit algorithm applied to the Eulerian equations, consumed 1500 seconds per cycle. Halving the reduced frequency would double the computer time requirement for the explicit scheme, since the time-step restriction remains essentially the same but the cycle is twice as long. On the other hand, the time step could probably be increased with the implicit scheme because the unsteady gradients would be smaller, and the time-step restriction is based on accuracy and not stability. So the implicit approach becomes relatively more efficient with decreasing frequency.

The implicit algorithm has been incorporated in a computer code, LTRAN2, a computational tool designed to assist the aerodynamicist in developing an understanding of the physics of unsteady transonic flows. Computed solutions from LTRAN2, for the linear version of the low-frequency equation, compare favorably with linear theory results, as shown in Figs. 3, 4, and 5. Good agreement in the nonlinear case has also been obtained in comparisons with the computed solutions of Magnus and Yoshihara (Fig. 6, 7, and 8). Finally, LTRAN2 solutions have been obtained for the three types of shock wave motion observed experimentally by Tijdeman (Figs. 6, 7, and 9).

References

[1] Ehlers, F. E., "A Finite Difference Method for the Solution of the Transonic Flow Around Harmonically Oscillating Wings," NASA CR-2257, 1974.

[2] Weatherill, W. H., Sabastian, J. D., and Ehlers, F. E., "On the Computation of the Transonic Perturbation Flow Fields Around Two- and Three-Dimensional Oscillating Wings," AIAA Paper 76-99, Jan. 1976.

[3] Traci, R. M., Farr, J. L., and Albano, E., "Perturbation Method for Transonic Flow About Oscillating Airfoils," AIAA Paper 75-877, June 1975.

[4] Traci, R. M., Albano, E. D., and Farr, J. L., "Small-Disturbance Transonic Flows About Oscillating Airfoils and Planar Wings," AFFDL-TR-75-100, June 1975.

[5] Ballhaus, W. F. and Goorjian, P. M., "Computation of Unsteady Transonic Flows by the Indicial Method," AIAA Paper 77-447, March 1977. To appear in *AIAA Journal*.

[6] Beam, R. M. and Warming, R. F., "Numerical Calculations of Two-Dimensional, Unsteady Transonic Flows with Circulation," NASA TN-D-7605, 1974.

[7] Beam, R. M. and Warming, R. F., "An Implicit Finite-Difference Algorithm for Hyperbolic Systems in Conservation-Law Form," *Journal of Computational Physics*, Vol. 22, 1976, pp. 87-110.

[8] Magnus, R. J. and Yoshihara, H., "Calculations of Transonic Flow Over an Oscillating Airfoil," AIAA Paper 75-98, Jan. 1975.

[9] Ballhaus, W. F. and Lomax, H., "The Numerical Simulation of Low Frequency Unsteady Transonic Flow Fields," *Lecture Notes in Physics*, Springer-Verlag, Vol. 35, 1975, pp. 57-63.

[10] Ballhaus, W. F. and Steger, J. L., "Implicit Approximate-Factorization Schemes for the Low-Frequency Transonic Equation," NASA TM-X-73,082, Nov. 1975.

[11] Beam, R. M. and Ballhaus, W. F., "Numerical Integration of the Small-Disturbance Potential and Euler Equations for Unsteady Transonic Flow," NASA SP-347, Part II, March 1975, pp. 789-809.

[12] Ballhaus, W. F., Magnus, R., and Yoshihara, H., "Some Examples of Unsteady Transonic Flows over Airfoils," *Proceedings of the Symposium on Unsteady Aerodynamics*, Vol. II, University of Arizona, 1975, pp. 769-791.

[13] Caradonna, F. X. and Isom, M. P., "Numerical Calculation of Unsteady Transonic Potential Flow over Helicopter Rotor Blades," *AIAA Journal*, Vol. 14, 1976, pp. 482-488.

[14] Ballhaus, W. F., "Some Recent Progress in Transonic Flow Computations," *VKI Lecture Series: Computational Fluid Dynamics*, von Karman Institute for Fluid Dynamics, Rhode-St-Genese, Belgium, March 15-19, 1976.

[15] Magnus, R. and Yoshihara, H., "The Transonic Oscillating Flap," AIAA Paper 76-327, July 1976.

[16] Ballhaus, W. F., Bailey, F. R., and Frick, J., "Improved Computational Treatment of Transonic Flow about Swept Wings," *Proceedings of the 13th Annual Meeting of the Society for Engineering Science, Inc.*, NASA CP-2001, Nov. 1976.

[17] Tijdeman, H., "On the Motion of Shock Waves on an Airfoil with Oscillating Flap," *Symposium Transsonicum II*, Springer-Verlag, 1975, pp. 49-56.